Massive mobilization of toxic elements from an intact rock glacier in the Central Eastern Alps: insights into ice melt dynamics

Hoda Moradi[1,*], Gerhard Furrer[2], Michael Margreth[3], David Mair[1], Christoph Wanner[1]

[1]Institute of Geological Sciences, Department of Earth Sciences, University of Bern, Baltzerstrasse 3, CH-3012 Bern, Switzerland
[2]Institute of Biochemistry and Pollutant Dynamics (IBP), Department of Environmental Systems Science, ETH Zurich, CH-8092 Zurich, Switzerland
[3]Swiss Federal Institute for Forest, Snow and Landscape Research WSL, Mountain Hydrology and Mass Movements, Zürichstrasse 111, CH-8903 Birmensdorf, Switzerland

Correspondence to: Hoda Moradi (hoda.moradi@unibe.ch)

Abstract. In the Central Eastern Alps, an increasing number of high-altitude streams display high concentrations of toxic solutes such as Al, F^-, Mn, and Ni that may strongly exceed drinking water limits. Previous studies have shown that these elements are mobilized from rock glaciers occurring at the origin of the streams. This is caused by the weathering of pyrite producing sulfuric acid and therefore promoting the leaching of these elements from the crystalline host rocks. After mobilization, the elements are temporally stored and enriched in the rock glacier ice. Today, the climate-change-induced accelerated melting of rock glaciers thus leads to a quick and focused export in summer when ice melt export rates are high. The temporal storage of mobilized elements in the rock glacier ice opens up the opportunity to use the strong chemical signal in the streams to track rock glacier melt dynamics and to identify the governing processes controlling the export of ice melt. To test this and to assess the consequences of accelerated rock glacier melt on streamwater quality, here we present a two-year dataset (2021, 2022) of monitoring a high-alpine stream originating from an intact rock glacier located in Eastern Switzerland. The monitoring includes monthly sampling and discharge measurements at the rock glacier outlet, as well as continuous tracking of the geogenic fluxes of toxic solutes using a pressure and conductivity probe. Our monitoring revealed high annual fluxes with strong seasonal variation, whereby the fluxes were highest during the warm summer months. In 2021, the annual fluxes were up to several tons each, which is remarkable given that the area of the rock glacier covers only about 40'000 m^2. Interestingly, in 2022 the fluxes were about 30 % lower despite the record-high summer temperatures. A similar difference was observed for the annual discharge recorded for the two years. This suggests that the export of both ice melt and toxic solutes are strongly controlled by the amount of water from snowmelt and precipitation infiltrating into the rock glacier system. The dry weather and low discharge rates in 2022 thus likely lead to lower export rates compared to 2021, when snow height and precipitation rates were above average. Nevertheless, in both monitoring years the degradation of the rock glacier significantly contributed to the discharge of the downhill stream. Based on these aspects, we present conceptual models for accumulation of toxic solutes in rock glacier ice well as for their water driven mobilization during accelerated rock glacier degradation. Finally, we argue that monitoring solute fluxes exported from rock glaciers is a

promising future research direction for obtaining more reliable estimates of the amount of ice melt exported from rock glaciers.

1 Introduction

Rock glaciers contain valuable long-term freshwater resources and are thus important for high-alpine water budgets (Jones et al., 2018; Wagner et al., 2021). Rock glaciers are tongue shaped high-alpine landforms of poorly sorted, angular-rock debris and ice. They can move as a result of the deformation of internal ice leading to a gravity-driven creep of these landforms (Jones et al., 2019; Giardino and Vitek, 1988; Barsch, 1996). The internal structure of active rock glaciers is composed of two fundamental components. Firstly, there is the active layer (AL), which is usually several decimeters to a few meters thick. Secondly, beneath the active layer, there is a core of ice-supersaturated debris (non-glacial) and pure ice (glacial), as described by Ballantyne (Ballantyne, 2018). If all ice has melted, rock glaciers stop to creep and are classified as relict (Jones et al., 2018, 2019). The current inventory of global rock glacier water volume equivalent has been recently estimated to 83.2 ± 16.64 Gt, representing about 2 ‰ of the water volume equivalents stored in glaciers when excluding high-latitude cold regions (Jones et al., 2018). Because rock glaciers are more resilient to climatic fluctuations than mountain glaciers, the rapid retreat of the latter will increase the role of rock glacier as freshwater storage with ongoing climate change (Jones et al., 2019 and references therein; Li et al., 2024). This is manifested by the observation that in arid regions with only few mountain glaciers such as North Asia, the ratio between water equivalents stored in rock glaciers and those stored in glacier is up to 4 % (Jones et al., 2018). A regional study conducted in Austria even proposed a water equivalent ratio of about 1:12 (8.3 %) for rock glacier versus glacier ice (Wagner et al., 2021a). To evaluate the contribution of rock glaciers to the hydrological system, it is essential to measure the discharge of meltwater into the hydrological system (Mark and Mckenzie, 2007).

Despite the increasing importance of intact rock glaciers for the hydrology of high mountainous areas, little is known to date regarding ice melt export in rock glaciers; in particular, how much this contributes to the discharge of mountainous streams. Geophysical methods including ground penetrating radar (GPR), electrical resistivity tomography (ERT), and refraction seismic tomography (RST) are typically applied to elucidate the internal structures of rock glaciers (Hauck, 2013; and references therein). For instance, Mewes et al. (2017) combined ERT and RST inversions to visualize the summer ice loss in the Bec de Bosson rock glacier in Switzerland. Furthermore, Hauck et al. (2011) verified the effectiveness of utilizing tomographic electrical and seismic imaging techniques to quantify contributions of ice, water, and air in permafrost regions and identify solid bedrock. None of these geophysical methods, however, allows to estimate contribution of meltwater from rock glacier to the downhill mountainous streams during ice melt season. Nevertheless, Krainer et al. (2015) estimated a yearly ice volume loss of 10,000 m³ for the Lazaun rock glacier in Southern Tyrol, Italy, corresponding to the uppermost 10 cm of the frozen rock glacier core, using differential GPS measurements combined with information obtained from two drill

65   cores of this rock glacier. Subsequently, they compared this volume to the discharge continuously measured downstream of a
       spring discharging form the rock glacier. This resulted in an estimated yearly average contribution of ice melt on the
       discharge of 0.6 L s^{-1}, which corresponded to about 2 % of the discharge from the entire rock glacier. The apparent little
       contribution of ice melt from the rock glacier to the total discharge demonstrates that these discharges represent a mixture of
       various water sources including rainwater, snowmelt, ice melt, and longer stored groundwater (Jones et al., 2019; Wagner et

70   al., 2021b). To differentiate between the different water sources, a significant number of hydrological studies have
       continuously monitored rock glaciers springs by performing measurements of parameters including discharge, electrical
       conductivity, stable isotopes (i.e. δ^{18}O, δ^2H values), and dissolved solutes (Williams et al., 2006; Krainer et al., 2007;
       Brighenti et al., 2021; Wagner et al., 2021a,b; Munroe and Handwerger, 2023). Most of these studies provided estimates for
       seasonally variable relative contributions of the different discharge components. However, since all of them utilized stable

75   isotope data, the rather strong seasonal variations of snowmelt and rainwater δ^{18}O and δ^2H values form a significant
       challenge for quantifying ice melt export rates using stable isotope data (Wanner et al., 2023b). Moreover, in case of the
       "Innere Ölgrube" rock glacier, the discharge from the rock glacier also contains a contribution from an uphill mountain
       glacier, which could not be differentiated from the ice melt being exported in the rock glacier (Wagner et al., 2021a).

80   Although rock glaciers may become more important for the drinking water supply of high-alpine regions (Jones et al., 2019;
       Wagner et al., 2020; 2021b), the anticipated increase in ice melt export rates may cause serious environmental challenges. In
       regions with pyrite-bearing and carbonate-free bedrock such as in the Central Eastern Alps, an increasing number of high-
       altitude streams originating from intact rock glacier display high concentrations of toxic solutes such as aluminum, nickel,
       manganese, and fluoride that may strongly exceed drinking water limits (Thies et al., 2007; Ilyashuk et al., 2014; Wanner et

85   al., 2023a). Outside the European Alps, the same is observed for instance downstream of permafrost areas in the Pyrenees in
       Spain (Zarroca et al., 2021) or the Rocky Mountains in the US (Todd et al., 2012). It follows that elevated solute
       concentrations in water draining from permafrost areas is a global phenomenon (Colombo et al., 2018; Brighenti et al.,
       2019). The adverse water quality of rock glacier springs is often caused by acid rock drainage (ARD) where the weathering
       of pyrite produces sulfuric acid and therefore promotes the leaching of toxic elements from the crystalline host rocks

90   (Wanner et al., 2018; 2023a). After mobilization, the elements are temporally stored and enriched in the rock glacier ice
       (Nickus et al., 2023). As a consequence, today the climate-change induced accelerated melting of rock glaciers leads to a
       quick and focused export in summer when ice melt production rates are high (Wanner et al., 2023a).

       The strong chemical signal in streams originating from intact rock glaciers affected by ARD due to the temporal storage of
95   mobilized elements in rock glacier ice may open up the opportunity to track rock glacier ice melt dynamics, their
       streamwater contribution, and to identify the governing processes. The opportunity occurs because under ARD conditions,
       all solutes measured downstream of rock glaciers almost exclusively originate from the rock glacier ice. In contrast, their
       concentration in snowmelt and rainwater is negligible. To test this approach and to further assess the consequences of

accelerated rock glacier melt on the stream water quality, we have initiated a detailed monitoring of a high alpine catchment
100   in the Central Eastern Alps in Switzerland. Here we present monitoring results for the years 2021 and 2022 with a particular
focus on toxic element fluxes being exported from the intact rock glacier at the origin of the catchment. The strong
seasonality of the fluxes with extreme values exceeding 100 kg per day during the hot summer months confirm the close link
between element fluxes and ice melt export rates. Consequently, the collected data provide novel insights on the coupled
thermal-hydraulic-chemical processes controlling the discharge and water quality of high-alpine streams originating from
105   intact rock glaciers. In the context of global warming, this information is key to assess the role of intact rock glaciers for the
future water budget in high-alpine streams as well as the associated environmental hazard caused by ARD in such systems.

2 Site description

Our flux monitoring is set up along the Aua da Prasüra mountain stream located in the Val Costainas valley in the Eastern
part of Switzerland, close to the Swiss-Italian border (Fig. 1a). The monitored catchment encompasses a remote area of 9.41
110   km^2 at an altitude ranging from 1800 to 2800 m a.s.l with no mining and almost no other anthropogenic activities apart from
a small area that is used as cattle pasture during summertime. Geologically, the area is part of the crystalline basement of the
Austroalpine nappes (Schmid et al., 2004). These basement nappes are free of carbonate rocks and mostly consist of mica-
rich, strongly weathered paragneiss and quartz-rich orthogneiss (swisstopo, 2024; Schmid, 1973). Quaternary deposits,
consisting of material from these units such as moraines and alluvial cones, cover a substantial part of the study area. In
115   addition, both intact and relict rock glaciers are frequently found in the catchment. The Aua da Prasüra stream itself
originates from three springs (AP1, AP2, and AP3, Fig. 1) discharging from an ice-rich permafrost zone (Fig. 1b) with the
typical morphology of an intact rock glacier (Fig. 2). Based on the geological map of the catchment (Fig. 1a) as well as a
high-resolution digital elevation model resulting from UAV (uncrewed aerial vehicle) imagery (Fig. 2), the surface area of
the rock glacier at the origin of the stream is approximately 40,000 m^2 (Fig. 2).

120

As described previously in Wanner et al., (2023a), the three rock glacier springs show a typical acid rock drainage (ARD)
signature with pH values as low as 5.0, and concentrations of Al, F$^-$, Mn, and Ni exceeding the corresponding drinking water
limits by up to 2 orders of magnitude. The discharge from the rock glacier is highest at the spring discharging at the lowest
elevation (AP1, 2660 m a.s.l). While this spring is constantly discharging water, the two others, located at 2700 (AP2) and
125   2770 (AP3) m a.s.l., respectively, fell dry in late summer during all the monitoring years. Downstream of sampling location
AP5 (Fig. 1a), the pH and temperature of the stream increases to values above 5.5 and 5 °C, respectively, resulting in the
precipitation of nanocrystalline basaluminite (Al$_4$OH$_{10}$(SO$_4$) x (H$_2$O)$_5$) because of its strong pH- and temperature-dependent
solubility (Wanner et al., 2018, 2023a). The precipitation is visible as white coatings on the bedload of the stream (Fig. S1,
Supplement) until the outlet of the catchment, which is about 5 km downstream at an altitude of 1890 m a.s.l. at sampling
130   location AP10 (Fig. 1a). Based on historical aerial photographs, precipitation only occurs since the Year 2000 (Wanner et al.,

2023a). This observation serves as a strong indicator of a significant decline in water quality of the monitored stream over the past 30 years.
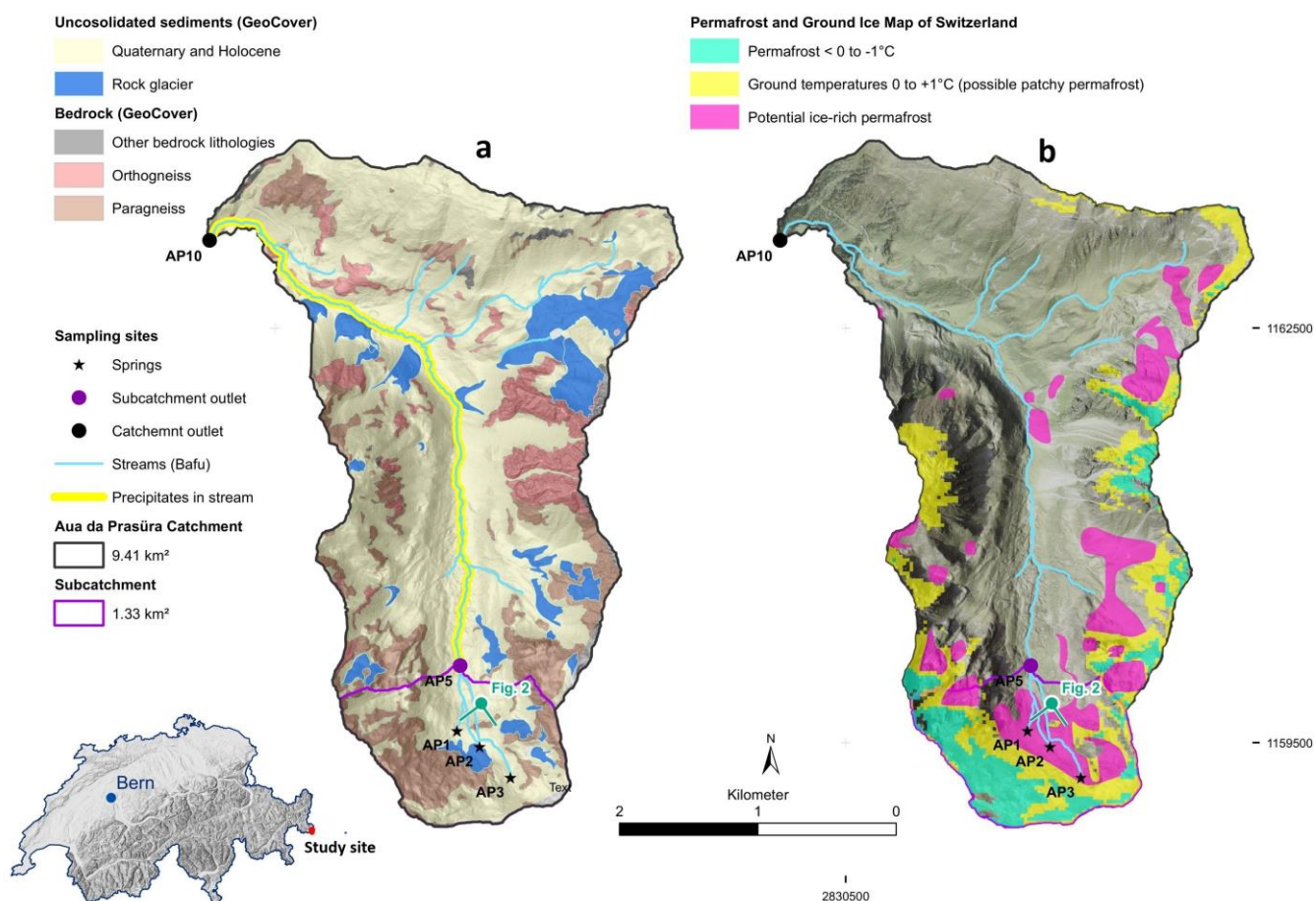
Figure 1: Val Costainas (a) Geological map modified from the GeoCover (© swisstopo) dataset from the Federal Office of Topography swisstopo (adapted from swisstopo, 2022) **based on field observations, and (b) permafrost and ground ice map of the Aua da Prasüra catchment** (Kenner et al., 2019). **The star symbols refer to the locations of the three rock glacier springs at the origin of the catchment (AP1, AP2, and AP3), whereas the filled circles refer to the two sampling locations downstream of the rock glacier (AP5, AP10). The area of the catchment at the upstream location at AP5 is 1.33 km², corresponding to about 14 % of the catchment sampled at the downstream AP10 location (catchment area = 9.41 km²) where a pressure and conductivity probe is installed. The green circle with the two tips illustrates the location and direction of the UAV for taking the photograph of the rock glacier shown in Figure 2. The section of the stream with white-coated bedload coatings (i.e. basaluminite, Fig. S1, Supplement) is highlighted in yellow. Basemaps: SwissAlti3D digital elevation model and SWISSIMAGE (© swisstopo).**
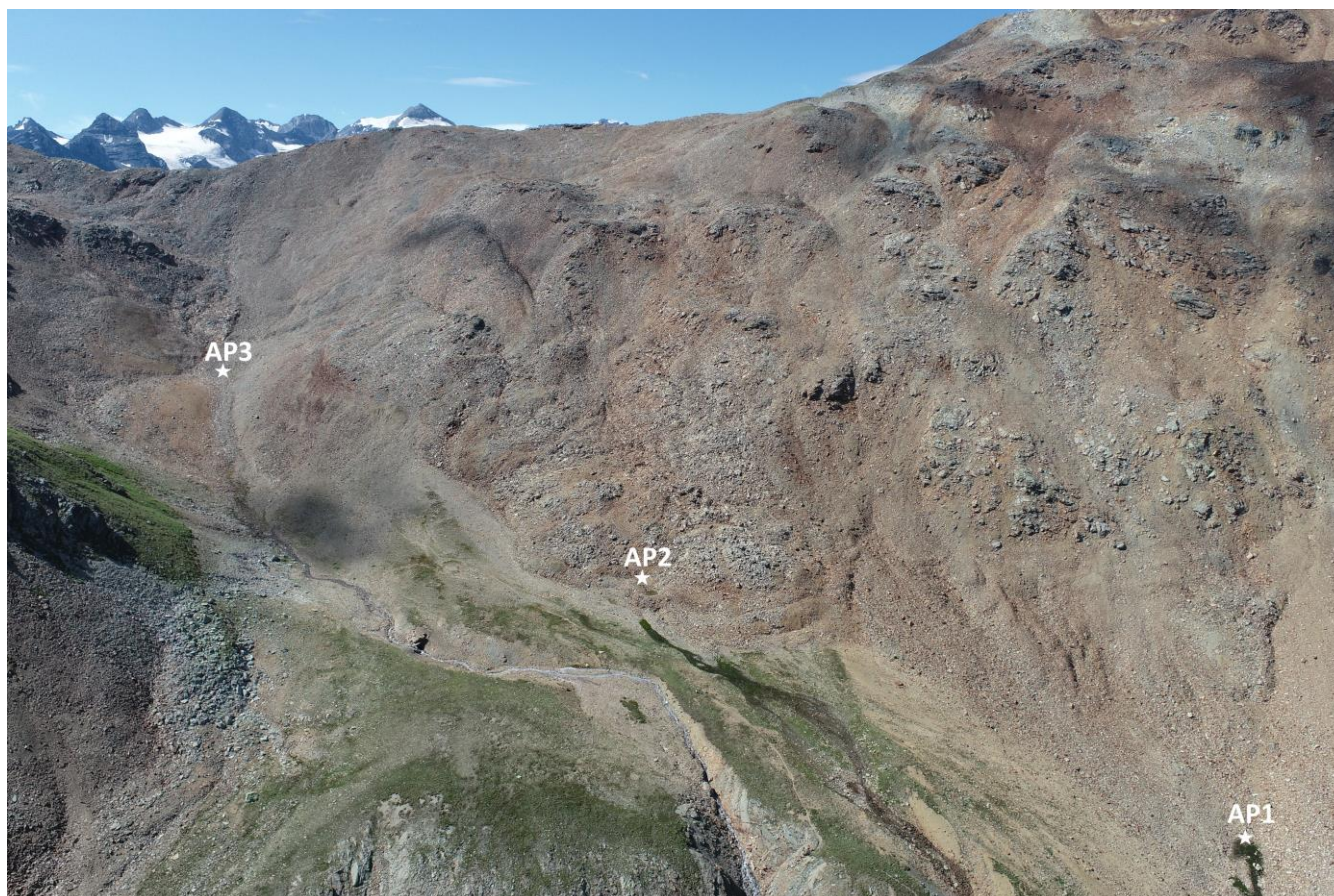
Figure 2: UAV photograph of the entire rock glacier with the three rock glacier springs AP1-AP3.

3 Methods

The main aim of our monitoring is to continuously track the fluxes of toxic elements being transported in the Aua da Prasüra stream. To relate these to the fluxes being exported from the intact rock glacier at the origin of the stream, we chose two monitoring locations. The first one is located at the merging point of the three rock glacier springs at location AP5, the second one about 5 km downstream of the rock glacier at AP10 (Fig. 1). With a catchment size of 1.33 m^2, location AP5 corresponds to 14 % of the catchment size monitored at AP10 (catchment area = 9.41 m^2).

The monitoring includes the collection and analyses of streamwater samples, as well as manual and automated measurements of the stream discharges as detailed below. Because of the presence of large rock boulders, the seasonally low discharge, and the potential relevance of hidden subsurface flow, reliable discharge and flux measurements at the three rock glacier springs are impossible (AP1, AP2, and AP3, Fig. 1).

3.1 Sampling of streamwater

Streamwater samples were collected from five different locations: AP1, AP2, AP3, AP5, and AP10 (Fig. 1). Sampling took
160   place between May and October of 2021 and 2022, with different sampling intervals. At the most downstream and hence
best accessible location at AP10, samples were collected biweekly and also outside the May to October period. In the source
region, AP1 and AP5, corresponding to the rock glacier spring with the highest discharge and the merging point of all three
rock glacier springs, respectively, sampling was carried out approximately every 1.5 months. The two additional rock glacier
springs (AP2, AP3) could only be sampled sporadically because they usually fall dry after termination of the snowmelt in
165   late summer. For all samples, pH, electrical conductivity (EC), and water temperature were measured on-site using Hamilton
electrodes with Knick Portamess-913 field instruments. In addition, samples were filtered on-site using 0.2 µm filters and
stored in polyethylene bottles. For the analyses of major cations and trace elements, one aliquot per sample was acidified
using one drop of a 30 % HNO_3 solution. All samples were stored at 4 °C prior to analysis.

3.2 Discharge measurements

170   At the two main monitoring sites (AP5, AP10), the discharge of the stream was measured manually approximately every 1.5
months between May and October of 2021 and 2022. At AP10, discharge measurements were additionally performed in
early spring (March-April). These measurements were carried out with the Sommer TQ-S Tracer System using the well-
established tracer-dilution method with NaCl as tracer (e.g. Calkins and Dunne, 1970; Day, 1977; Leibundgut et al., 2009).
The Tracer System consists of two electrical conductivity probes connected via Bluetooth to the Software TQ-Commander.
175   For each site, the probes were calibrated with streamwater samples, allowing the calculation of NaCl concentrations based
on electrical conductivity values (calculation is executed automatically by the software). When a fixed quantity of NaCl is
added upstream, the system automatically quantifies the discharge based on the NaCl concentrations registered at the
measurement site (integral of concentration curves). For each discharge quantification, we executed two measurements by
using different amounts of salt, resulting in four measurements in total. The reported discharge values constitute the average
180   of these four measurements. Based on the spread of the measurements, the uncertainty of the discharge quantification was
well within ±5 %, which is consistent with the maximum measurement uncertainty estimated by the producer company
(Sommer). In general, the uncertainty of discharge measurements using the salt dilution method depends on calibration, the
amount of used salt and on the measurement setup, i.e. the length of mixing section. The better the salty water is mixed with
the stream water, the higher the accuracy of measured discharge values. These aspects were taken into account during the
185   measurements.

3.3 Automatic water table and electric conductivity measurements

At the AP10 location, the Canton of Graubünden operates a combined water table, temperature and conductivity probe. The probe takes a measurement of these parameters every ten minutes and the data are published online in real time (ANU, 2023). During wintertime, the discharge of the stream is very low, and the stream is periodically covered by snow and an ice layer rendering the readings of the probe unreliable. With the beginning of the snowmelt season in spring, the discharge increases, and the data recorded by the probe becomes more reliable. Based on our observations, we consider the recorded data from May to October to be reliable, and we exclusively utilize these measurements for analysis. Nevertheless, even in summertime, loss of data occurred. To overcome this problem, different approaches were applied. In the event of water table data loss, the data were handled differently based on the circumstances. In regular situations without any notable meteorological events, a linear interpolation method was employed to reconstruct the missing data. If the data loss occurred immediately after a precipitation event, a typical recession curve equation (Maillet, 1905) was used:

$$Q_t = Q_0\, e^{-at} \tag{1}$$

Where Q_t is the flow rate at time t, Q_0 is the maximum flow rate during the precipitation event, and a is the fitting parameter used to match the date, collected after the data recording had been resumed. A slightly different approach was used in the event of electrical conductivity measurement problems to reconstruct for the missing data. Since we used these data to estimated solute concentrations (see below), the chemical analyses of the biweekly samples were used to ensure the continuity of the concentration estimates via linear interpolation during such events. Based on the comparison with manual discharge and conductivity measurements, the uncertainty of the automated water table and electric conductivity measurements were estimated to ±1 cm and ±5 %, respectively.

3.4 Analytical methods

3.4.1 Water analysis

Concentrations of major cations and anions, Na^+, K^+, Ca^{2+}, Mg^{2+}, NH_4^+, F^-, Cl^-, Br^-, NO_3^-, SO_4^{2-}, of the streamwater samples were measured by ion chromatography (IC) at the University of Bern using a Metrohm 850 system with a detection limit of 0.1 mg L^{-1} for cations and 0.016 mg L^{-1} for anions. Total inorganic and organic carbon concentrations were determined using a TIC/TOC analyzer (Analytic Jena multi N/C 2100S) with detection limits of 0.1 mg L^{-1} for inorganic and 0.5 mg L^{-1} for organic carbon. Inductively coupled plasma optical emission spectroscopy (ICP-OES) with a Varian 720-ES ICP spectrometer was used to determine aqueous concentrations of Al, Ba, Cu, Fe, Mn, Ni, Zn, Si, Sr, Pb and Cd. The detection limit was 1 µg L^{-1} for Ba, Mn, Sr and Zn, 3 µg L^{-1} for Al and Si, 5 µg L^{-1} for Fe, Ni, Cd and Cu, and 20 µg L^{-1} for Pb. Concentrations of As were determined by atomic adsorption spectroscopy (AAS) using a ContrA 700 (Analytik Jena) with a detection limit of 4 µg L^{-1}. The analytical error of all these measurements was ±5%.

3.5 Determination of fluxes

220   At the two main monitoring sites (AP5, AP10), discharge measurements were carried out right after collecting streamwater samples. Accordingly, the fluxes of solutes (e.g. in mg s^{-1}) correspond to the product of their concentrations (e.g. in mg L^{-1}) and the measured discharge (e.g. in L s^{-1}). Between May and October of 2021 and 2022, our data thus allow determining solute fluxes every 1.5 months. In addition to these sporadic flux determinations, we have continuously estimated the fluxes of solutes at the downstream location (AP10) using the continuous water table and electrical conductivity data collected by

225   the installed probe. To do so, water table measurements were correlated with discharge measurements to obtain a discharge-water table relationship (rating curve) allowing to continuously determine the discharge. Likewise, the electrical conductivity measurements were correlated with solute concentrations measured on the biweekly water samples to establish a conductivity-concentration relationship for the continuous determination of solute concentrations. The product of these two determinations resulted in daily averages of solutes fluxes. In this study, we focus on the fluxes of Al, F^{-}, Zn, Mn, and Ni

230   because these solutes are of the highest environmental concern in streams affected by ARD in the Central Eastern Alps (Wanner et al., 2023a). Taking into account the errors of the individual measurements (discharge, electrical conductivity, element concentrations) used for the continuous flux estimations, the uncertainty was estimated to be within ±10 %.

4 Results

4.1 Discharge measurements

235   #### 4.1.1. Intermittent discharge measurements at AP5 and AP10
The intermittent discharge measurements at the two monitoring locations showed strong seasonal variations (Table 1). The highest values above 200 L s^{-1} (AP5) and 1000 L s^{-1} (AP10) were measured during snowmelt in late spring or early summer (May-July). At AP10, the lowest discharge (< 70 L s^{-1}) was recorded in early spring (Mar-Apr) when winter recession of discharge ends before snow melt period starts. Owing to the high altitude, no sampling was possible at AP5 at this time.

240   Accordingly, at AP5 the lowest discharge (<30 L s^{-1}) was measured in early fall in both monitoring years.

In addition to the seasonal discharge variations, also the ratio of the discharge at the two monitoring sites strongly varied (Table 1). With the exception of the peak snowmelt period captured on 10 June 2021, the discharge at AP5 relative to that at AP10 was always higher than the 14 % expected from the difference in the corresponding catchment areas. In both

245   monitoring years, the ratio peaked with values above 30 % right after the termination of the snowmelt in early July and hence up to 3 times higher than expected from the two catchment sizes. During low discharge conditions in fall, the relative discharge at AP5 was still slightly below 20 % and hence at least 1.3 times higher than expected from the area of the two catchments.

Table 1: Discharge measurements at the two monitoring locations and relative discharge contribution of the upstream catchment at AP5 on the discharge of the entire catchment at AP10 (Fig. 1). Also shown is the relative discharge contribution AP5/AP10 normalized by the ratio of the two catchment areas (AP5: 1.33 km^2; AP10: 9.41 km^2), to illustrate that the discharge from the upstream catchment and hence the rock glacier at the source of the stream is disproportionately high.

Date	Discharge at AP10 (L s^{-1})	Discharge at AP5 (L s^{-1})	Relative discharge contribution AP5/AP10 (%)	Relative discharge contribution AP5/AP10 normalized by the ratio of the two catchment areas (1.33/9.41)
23 March 2021	53	n.m.	-	-
10 June 2021	1116	153	14	1
8 July 2021	629	269	43	3
18 August 2021	384	58	5	1.1
22 September 2021	136	26	19	1.4
21 October 2021	182	34	18	1.3
2 April 2022	64	n.m.	n.m.	n.m.
20 May 2022	733	n.m.	n.m.	n.m.
5 July 2022	306	91	30	2.1
13 August 2022	203	47	23	1.6
11 October 2022	140	27	19	1.4

n.m.: No measurement possible

4.1.2 Continuous discharge measurements at AP10 (downstream location)

The water table-discharge correlation obtained for the downstream location at AP10 is shown in Fig. 3. Above a discharge of ca. 60 L s^{-1}, the data nicely follow a polynomial correlation. Nevertheless, we consider discharge estimates below 100 L s^{-1} as unreliable because this is exclusively the case in winter when the stream is partially and periodically covered by ice and snow, strongly affecting the hydraulics (i.e. the relevant cross section of the stream) at the measurement location. Thus, for 2021 and 2022 continuous discharge estimates are only used for the period between May and October. The continuous discharge data are presented with the seasonal flux estimates below.
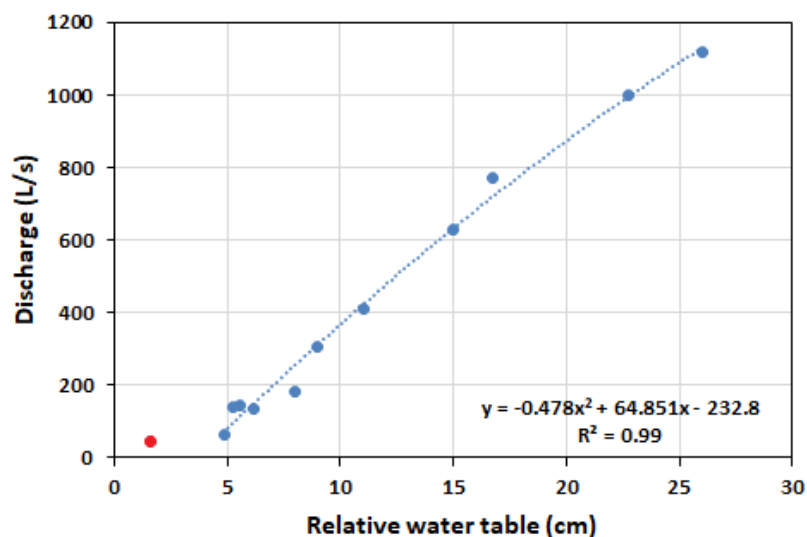
Figure 3: Correlation between water table and manual discharge measurements at the AP10 location and the derived polynomial correlation for water tables above 5 cm. At lower water tables, the correlation does not work, likely because such low values are observed in wintertime, when the hydraulics at the measurement location are strongly affected by ice This is manifested by the measurements conducted on 23 March 2021, yielding a discharge of 53 L s⁻¹ (red dot).

4.2 Chemical composition of the streamwater

Table 2 presents the concentration range of selected solutes in streamwater samples collected from all five sampling locations. The full analyses are provided in the Supplement (Tables S1-S5). The temperature of the three rock glacier springs at the origin of the Aua da Prasüra stream (AP1, AP2, and AP3, Fig. 1) is constantly below 2 °C, confirming that all springs originate from an intact rock glacier containing ice (Fig. 2). At the rock glacier springs, the concentrations of Al, F⁻, Mn, and Ni are almost always above the corresponding drinking water limits. The highest concentrations are found at AP1, discharging at the lowest altitude (2660 m a.s.l., Figs. 1, 2). Here, the concentrations reach values up to 28.7 mg L⁻¹ Al, 23.1 mg L⁻¹ F⁻, 11.3 mg L⁻¹ Mn, and 3.3 mg L⁻¹ Ni. In case of Mn and Ni, these correspond to a very strong exceedance of the Swiss drinking water limit by factors of 226 and 165, respectively. For Al and F⁻, the situation is less severe, but the drinking water limits are still exceeded by factors of up to 143 and 15, respectively. At the other two rock glaciers springs (AP2, AP3), the concentrations are lower and decrease with increasing altitude (Table 2). For instance, the maximum concentration of Ni at AP2 (2700 m a.s.l.) and AP3 (2770 m a.s.l.) are 1.6 and 0.4 mg L⁻¹, respectively, and thus 2 and 8 times lower than at AP1. In contrast to the other solutes of interest, the Swiss drinking water limit for Zn (5 mg L⁻¹) is only periodically exceeded at the lowest rock glacier spring (AP1).

Downstream of the rock glacier springs, the temperature and pH gradually increase, while the solute concentrations decrease as manifested by the streamwater samples collected at AP5 and AP10 (Table 2). Nevertheless, 5 km downstream and at an altitude of 1890 m a.s.l., the concentrations of Mn (≤0.37 mg L^{-1}) and Ni (≤0.24 mg L^{-1}) at AP10 (Fig. 1) still exceed the
290   drinking water limits by a factor of up to 7 or 12, respectively.

Table 2: Chemical composition of streamwater samples from different locations along the Aua da Prasüra stream (Fig. 1)

Location	Number of samples	Altitude (m a.s.l.)	T (°C)	pH	EC (µs cm^{-1})	TDS (mg L^{-1})	Al (mg L^{-1})	Mn (mg L^{-1})	Ni (mg L^{-1})	Zn (mg L^{-1})	As (µg L^{-1})	F (mg L^{-1})	SO$_4$ (mg L^{-1})
AP1	5	2660	0.8-1.4	4.7-5.0	1197-2040	1819-3942	15.4-28.7	4.8-11.3	1.70-3.30	4.20-7.81	<4-4.1	2.1-23.1	1354-2803
AP2	5	2700	0.3-3.1	5.1-5.2	160-711	559-3083	2.7-10.9	0.3-3.4	0.35-1.63	0.74-2.49	<4	0.4-5.6	415-1986
AP3	6	2770	0.7-4.7	5.8-6.4	403-1625	519-1616	0.5-1.5	0.009-0.191	0.05-0.39	0.12-1.16	<4	1.4-4.3	369-1008
AP5	8	2530	1.4-8.9	5.3-5.7	317-1208	388-1689	1.4-8.3	0.079-1.729	0.18-1.22	0.56-3.01	<4	0.5-6.5	285-1287
AP10	39	1890	0.6-11.4	6.0-8.1	133-440	117-507	0.01-0.41	0.007-0.365	0.02-0.24	0.05-0.62	<4	0.5-1.8	80-327
[1]Drinking water limit							0.2	0.05	0.02	5	0.01	1.5	

[1]https://www.fedlex.admin.ch/eli/cc/2017/153/de

4.2.1 Seasonal variation of concentrations of toxic elements

At the downstream monitoring location AP10 (Fig. 1), the concentrations of Ni, Zn and F$^-$ show strong linear correlations with the electrical conductivity measured by the installed probe as evidenced by linear correlation coefficients (R^2) of at least 0.91 (Fig. 4). Accordingly, the conductivity data recorded by the probe allow to continuously estimating the concentrations of these three solutes using the derived linear calibration curves. For Mn and other reactive solutes such as Al, the correlation
300   between concentrations and conductivity values is poor (Fig. 4), which means that these concentrations cannot be estimated using the conductivity data.
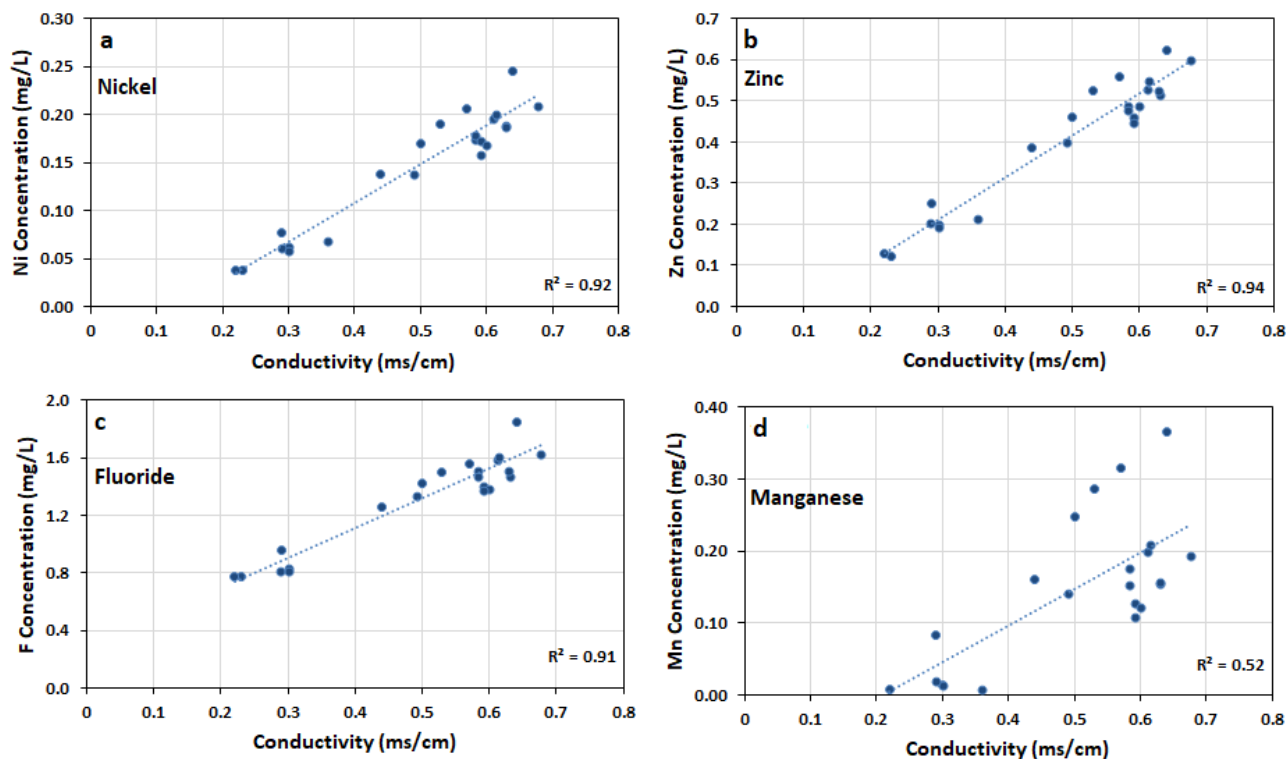
Figure 4: Linear correlations at the downstream monitoring location AP10 between electric conductivity (EC) measured by the installed probe and concentrations of selected solutes. (a) Ni (b) Zn (c) F⁻ (d) Mn.
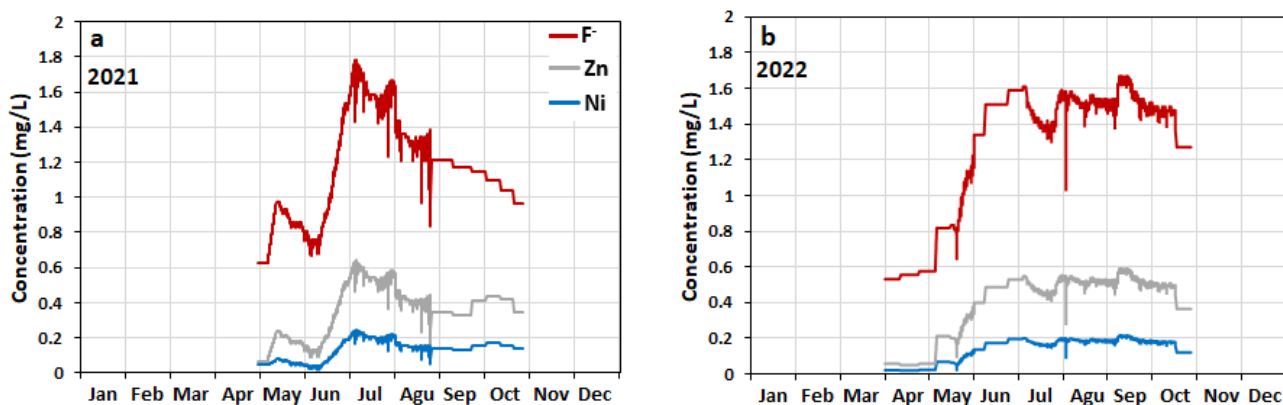
Figure 5: Seasonal evolution of the concentrations of F⁻, Zn, and Ni at the downstream monitoring location, AP10, estimated based on the electrical conductivity data and the correlations shown in Figure 4. (a) 2021, (b) 2022. Because of the unreliability of EC data, a linear interpolation of the chemical analysis of the biweekly samples (Table S1, Supplement) was employed for the following periods: 1–14. May 2021, 29. Aug–30. Oct 2021, 1–20. May 2022, 7. Jun–7. Jul 2022, and 21–30. Oct 2022.

315 Figure 5 illustrates the seasonal variations of the concentrations of F⁻, Zn, and Ni estimated based on the conductivity data and the correlations shown in Fig. 4. In both monitoring years, these solutes show maximum concentrations in summer although the seasonal behavior was slightly different in the two years. In 2021, the highest concentrations are estimated for early July followed by a gradual decrease until the end of the monitoring period at the end of October, except for short-term excursions where the concentrations periodically increased. In 2022, with the exception of short negative and positive

320 excursion, the concentrations were nearly constant between early July and mid-September. For both monitoring years, the concentrations at the end of the monitoring period were roughly twice as high as at the beginning of the monitoring period in May. In contrast to the downstream monitoring location AP10, at the upstream monitoring location AP5 as well as at the most frequently sampled rock glacier spring AP1, the concentrations of the solutes except F⁻ (Al, Ni, Zn and Mn) generally increased during the May-October monitoring period and the highest values were measured towards the end of the

325 monitoring period (Fig. 6).
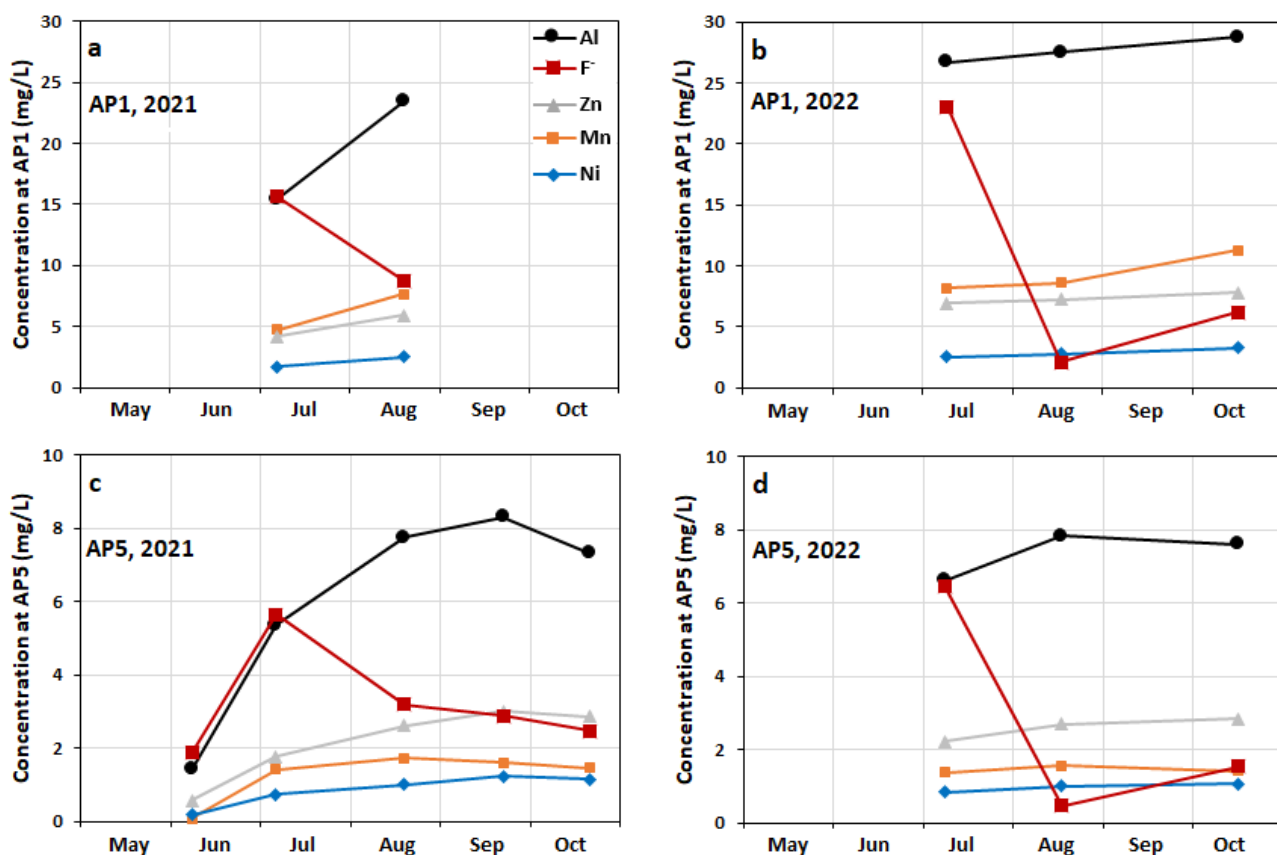
Figure 6: Seasonal variation of the concentrations of Al, F⁻, Zn, Mn, and Ni at the rock glacier spring AP1 and the upstream discharge monitoring location AP5 (Fig. 1). (a), (b) Concentrations of samples taken at AP1 in 2021 and 2022, respectively. (c), (d)

330 **Concentrations of samples taken at AP5 in 2021 and 2022, respectively.**

4.3 Seasonal evolution of mobilized fluxes

4.3.1 Manual flux measurements (AP5 and AP10)

At the two main monitoring locations AP5 and AP10 (Fig. 1), we took 8 and 10 flux measurements, respectively. Figure 7
335 presents the fluxes of Al, F⁻, Zn, Mn, and Ni. At both monitoring locations, these fluxes show a very similar pattern with a strong seasonal variation. In both years, the highest fluxes occurred in early July except for AP10, where in 2022 the maximum flux of F⁻ was observed in May. Among the five solutes, Al and F⁻ displayed the highest fluxes with values exceeding 100 kg per day at AP5 in July 2021. At the same sampling day, the fluxes of Zn, Mn, and Ni reached maximum values of 20-40 kg per day. In early and late summer, the fluxes were up to one order of magnitude lower.
340

At specific sampling dates, the two monitoring locations exhibited very similar fluxes for Zn and Ni. In contrast, the fluxes of Mn and Al are significantly lower at the downstream location (AP10), while the flux of F⁻ is slightly higher in fall when the discharge is low. This suggest that at AP10, only the fluxes of Zn and Ni may serve as a proxy for the processes occurring in the rock glacier at the source of the stream (see Discussion below).

345
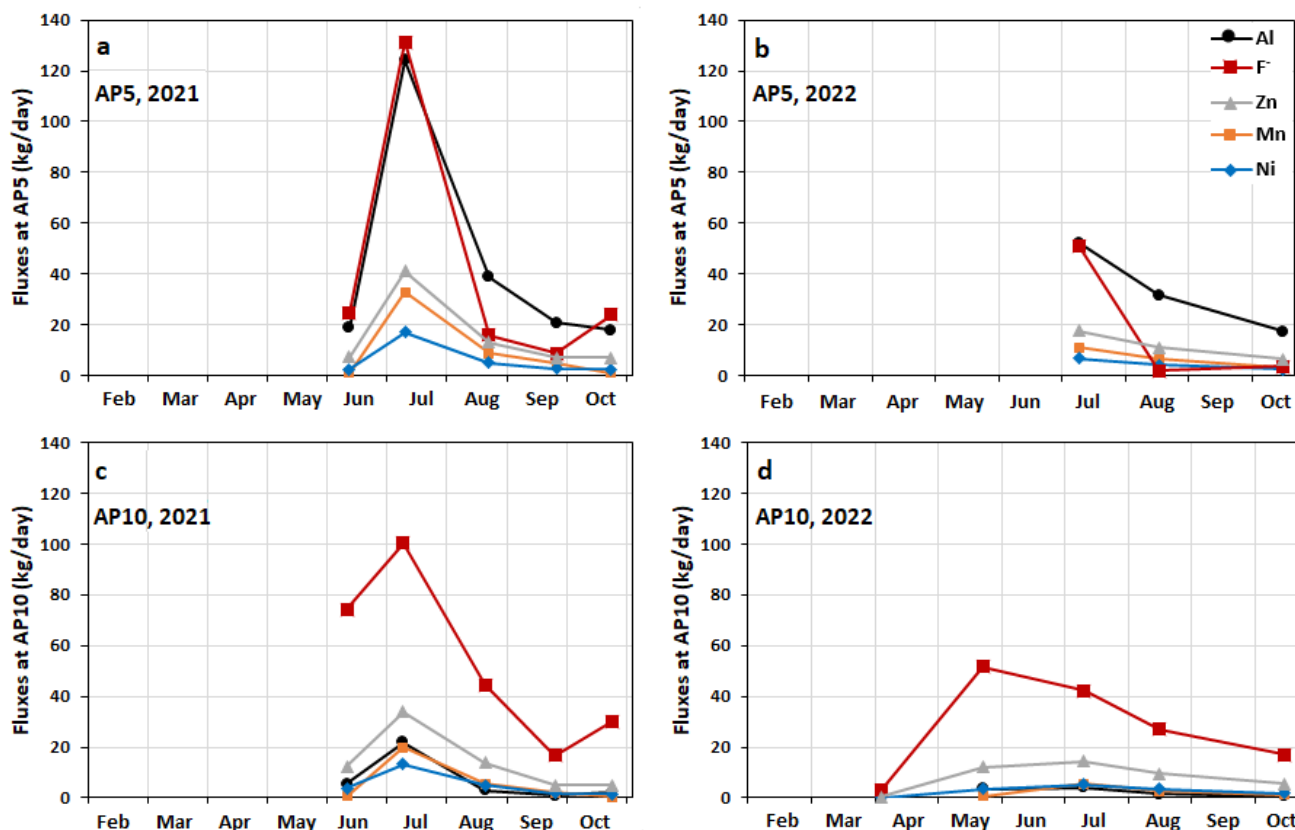
Figure 7: Fluxes of Al, F⁻, Zn, Mn, and Ni at the two main monitoring stations along the Aua da Prasüra stream. (a) Fluxes measured in 2021 at the upstream AP5 location. (b) Fluxes measured in 2022 at the upstream AP5 location. (c) Fluxes measured in 2021 at the downstream AP10 location. (d) Fluxes measured in 2022 at the downstream AP10 location.

4.3.2 Automatic flux estimation (AP10)

350

The fluxes of Zn and Ni continuously estimated at the downstream monitoring location AP10 are shown in Fig. 8. Integrating the fluxes for the 2021 monitoring period yields surprisingly high total fluxes of 2'570 and 940 kg for Zn and Ni, respectively. For the same period in 2022, the total fluxes for these two solutes were 1'830 and 650 kg, respectively, and hence 29-31 % lower than in 2021.

355

The seasonality of the estimated Ni and Zn fluxes is rather similar. In both monitoring years, the lowest values were observed at the beginning of the monitoring period in early May when the rock glacier at the origin of the stream was still covered by snow. During snowmelt, the increase in discharge is immediately followed by a rapid surge of the two fluxes, demonstrating that there is a very strong correlation between discharge and solute fluxes. Consequently, synchronous

360   discharge and flux peaks are observed during peak snowmelt conditions (Fig. 8a,b). In 2021, this was the case in mid-June. In 2022, the winter snow cover was less (Fig. 8c) and peak snowmelt conditions occurred about 3 weeks earlier at the end of May and the corresponding discharge and element fluxes were significantly lower than in 2021. After the snowmelt peaks, additional synchronous flux and discharge peaks occurred during heavy rainfall events. In 2021, this was the case in early July, early August, and early October (Fig. 8d). In 2022, such short-term discharge and flux peaks occurred in response to

365   precipitation events in early July, early August, mid-September and mid-October. In addition to the simultaneously occurring flux and discharge peaks (Fig. 8a,b), the strong correlation between the two parameters is also manifested by very similar patterns of their seasonal behavior in both monitoring years (Fig. 9).
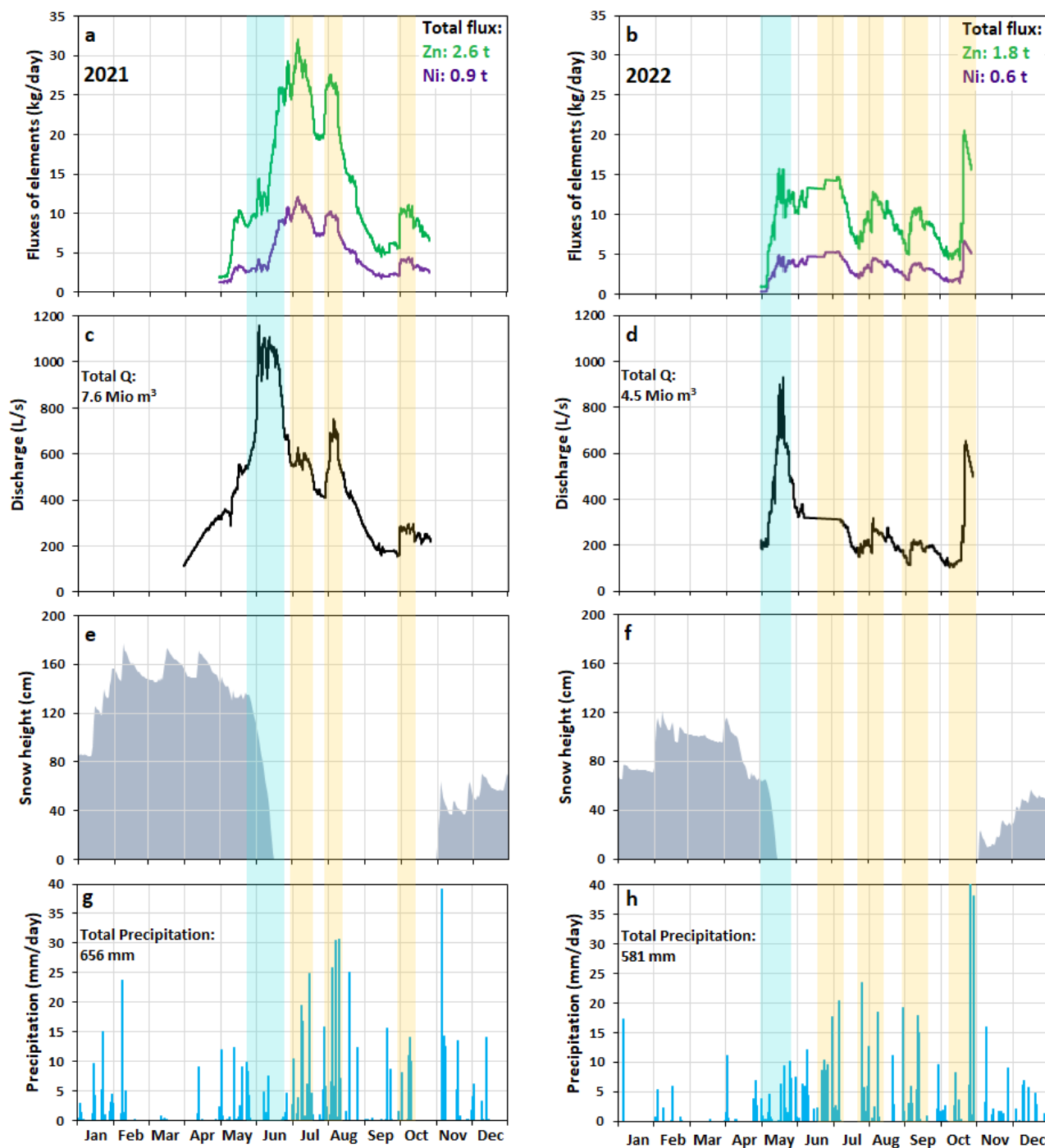
Figure 8: Seasonal evolution of key parameters recorded through the two monitoring years. (a), (b): Fluxes of Zn and Ni estimated at the downstream monitoring location AP10 (Fig. 1) in 2021 and 2022, respectively. (c), (d): Discharge of the Aua da Prasüra

stream measured at the same location in 2021 and 2022, respectively. (e), (f): Snow height recorded in 2021 and 2022 at the
Murtaröl snow station, located some 15 km Northwest of AP10 at an altitude of 2359 m a.s.l (SLF, 2023)**. (g), (h): Rainfall recorded**
375 **in 2021 and 2022 at the Santa Maria weather station, located some 6.5 km North of AP10 at an altitude of 1388 m a.s.l**
(MeteoSwiss, 2023)**. The light blue bars highlight synchronous discharge and flux peaks observed during snowmelt peak in June**
2021 and May 2022. The yellow bars mark synchronous peaks in discharge and element fluxes after precipitation events. Due to
technical problems, no reliable discharge data were obtained in June 2022. Therefore, a linear interpolation was used to retrieve
the data from June 7 to July 7. Technical problems also occurred from 24-31. October 2022 in response to a heavy rainfall event.
380 **For this event, a recession curve with Q_0 = 668 L s^{-1} and a = 0.00235 (eq. (1)) was applied to correct for the missing discharge data.**

5 Discussion

5.1 Tracking of toxic element fluxes exported from the studied rock glacier

The continuous monitoring of rock glacier springs is challenged by their remote location at high altitude and rugged
topography. In the studied system, however, the strong chemical signal allows to continuously track the concentrations of
385 conservatively behaving toxic solutes using a conductivity probe installed at a well accessible site, located ca. 5 km
downstream of the rock glacier at an altitude, which is about 800 m lower than the lowest rock glacier spring. This applies to
F$^-$, Zn and Ni as manifested by their strong linear correlations with the measured electrical conductivity (Fig. 4). For solutes
that do not behave conservatively such as Al and Mn, the correlation is poor (Fig. 4) and their concentrations cannot be
estimated using the conductivity data. In case of Al, this is because most of it precipitates as basaluminite along the stream as
390 manifested by the white-colored bedload downstream of AP5 (Fig S1, Supplement). Manganese behaves reactive because
the oxidizing conditions in the stream lead to a continuous oxidation and precipitation of Mn, originally mobilized by the
reduction of Mn oxides in the rock glacier at the origin of the stream (Wanner et al., 2023a). It follows that the concentration
of Mn at the downstream location AP10 is not only controlled by the mobilization in the rock glacier but also by the degree
of oxidation along the stream, which is a slow, kinetically-limited process (Diem and Stumm, 1984). The amount of Mn lost
395 due to oxidation along the stream thus strongly depends on the seasonally variable residence time of streamwater in the
monitored catchment, which is the reason why the correlation between concentration and conductivity is poor (Fig. 4).

Despite their conservative behavior, the seasonal concentration patterns for F$^-$, Zn and Ni vary along the stream (Figs. 5, 6).
The contrasting seasonal behavior of the concentrations near the rock glacier source (AP1, AP5, Fig. 6) and at the
400 downstream location (AP10, Fig. 5) is due to the fact that all concentrations are controlled by the amount of solutes being
mobilized from the rock glacier and the degree of dilution. Due to the strong difference in the catchment sizes at these three
sampling locations (AP1: 0.04 km^2, AP5: 1.33 km^2, AP10: 9.41 km^2), the degree of dilution by snowmelt and rainwater is
strongly different. Therefore, to quantitatively understand the seasonality of the mobilization of toxic elements from the rock
glacier, we propose that tracking the mobilized fluxes is more useful than element concentrations. This is because element

405 fluxes correspond to the product between element concentrations and the discharge and hence account for dilution effects by snowmelt and rainwater, which both show strong seasonal variations.

The conservative behavior of Zn and Ni along the stream is further manifested by the observation that at specific sampling dates, these solutes exhibit very similar fluxes at the two monitoring locations (Fig. 7). This eventually demonstrates that
410 monitoring the fluxes of Zn and Ni at the downstream monitoring location at AP10 allows tracking and assessing their mobilization from the rock glacier. Since the flux of F^- shows significant differences at the two monitoring locations (Fig. 7), its mobilization from the rock glacier cannot be fully tracked at the downstream monitoring location. This is because the tributaries merging with the main Aua da Prasüra stream downstream of the upper monitoring location at AP5 (Fig. 1) may also contribute to the F^- flux measured at AP10. This is particularly relevant at low flux conditions in spring and in fall
415 where the fluxes of F^- are usually higher at AP10 than at AP5 (Fig. 7).

Because of their reactive behavior, the total fluxes of Al, F^-, and Mn, exported from the rock glacier in each monitoring period can only be estimated based on the sporadic manual flux measurements carried out near the rock glacier outlet at AP5, their comparison with the fluxes of Zn and Ni not affected by any chemical reactions occurring along the stream (Fig. 7), and the total fluxes estimated for Zn and Ni estimated at AP10 (Fig. 8a). For Al and F^-, this yields annual fluxes of about
420 three times higher than those estimated for Zn (i.e. up to 10 t and 7 t in 2021 and 2022, respectively). For Mn, the annual fluxes exported from the rock glacier were likely in between those of Ni and Zn (2021: 940-2'570 kg; 2022: 650-1'830 kg).

5.2 Controls on element mobilization from intact rock glaciers: insights on ice melt export rates

The data collected along the Aua da Prasüra stream confirm that all toxic solutes showing elevated concentrations (e.g. Al, F^-
425 , Zn, Mn, and Ni) are predominantly mobilized from the intact rock glacier at the origin of the stream. Given that this rock glacier only covers an area of about 40,000 m^2 (Figs. 1, 2), the estimated total fluxes of 1–10 t per monitoring period (May-October) are quite striking and demonstrate that it operates as a strong and long-lasting chemical reactor. Moreover, the almost instantaneous response of the estimated fluxes to snowmelt and precipitation events in summer (Fig. 8) can only be explained if these elements are enriched and temporally stored in the rock glacier ice. Accordingly, the collected data
430 confirm that in geological settings affected by ARD, the interim storage of toxic elements in rock glaciers ice leads to a quick and focused export of toxic elements in summer when ice melt export rates are high (Wanner et al., 2023a). Because of their conservative behavior in the stream, the seasonal behavior of the fluxes of Ni and Zn are particularly useful to assess the controls on ice melt dynamics in the studied rock glacier and to estimate the corresponding ice melt export rates.

435 The very strong correlation between the flux and discharge curves (Figs. 8, 9), suggests that the amount of water infiltrating into the rock glacier system plays a crucial role in controlling the export of ice melt from the rock glacier. This is not only

manifested by the simultaneously occurring discharge and flux peaks (Fig. 8a,b) as well as the very similar behavior of the flux and discharge curves (Fig. 9), but also by the difference in the total discharge calculated for the two monitoring years. In 2022 when the total fluxes of Zn and Ni and consequently the export of ice melt from the rock glacier were about 30 %

440   lower than in 2021, the total discharge between May and October was 41 % lower than in 2021 (Fig. 8b). The lower discharge in 2022 resulted from the lower winter snow cover and the lower amount of precipitation in summer (Fig. 8). The apparently lower ice melt export rate in 2022 is remarkable given that 2022 corresponds to a year with record high temperature in the Alps (Noetzli, J. and Pellet, 2023), as manifested by much higher summer temperature than in 2021 (Fig. 9). Accordingly, in our study area the variable infiltration of water into rock glaciers caused by a varying winter snow cover

445   and variations in summer precipitation apparently has a much stronger effect on yearly ice melt export rates than the variation of the summer air temperature.

450
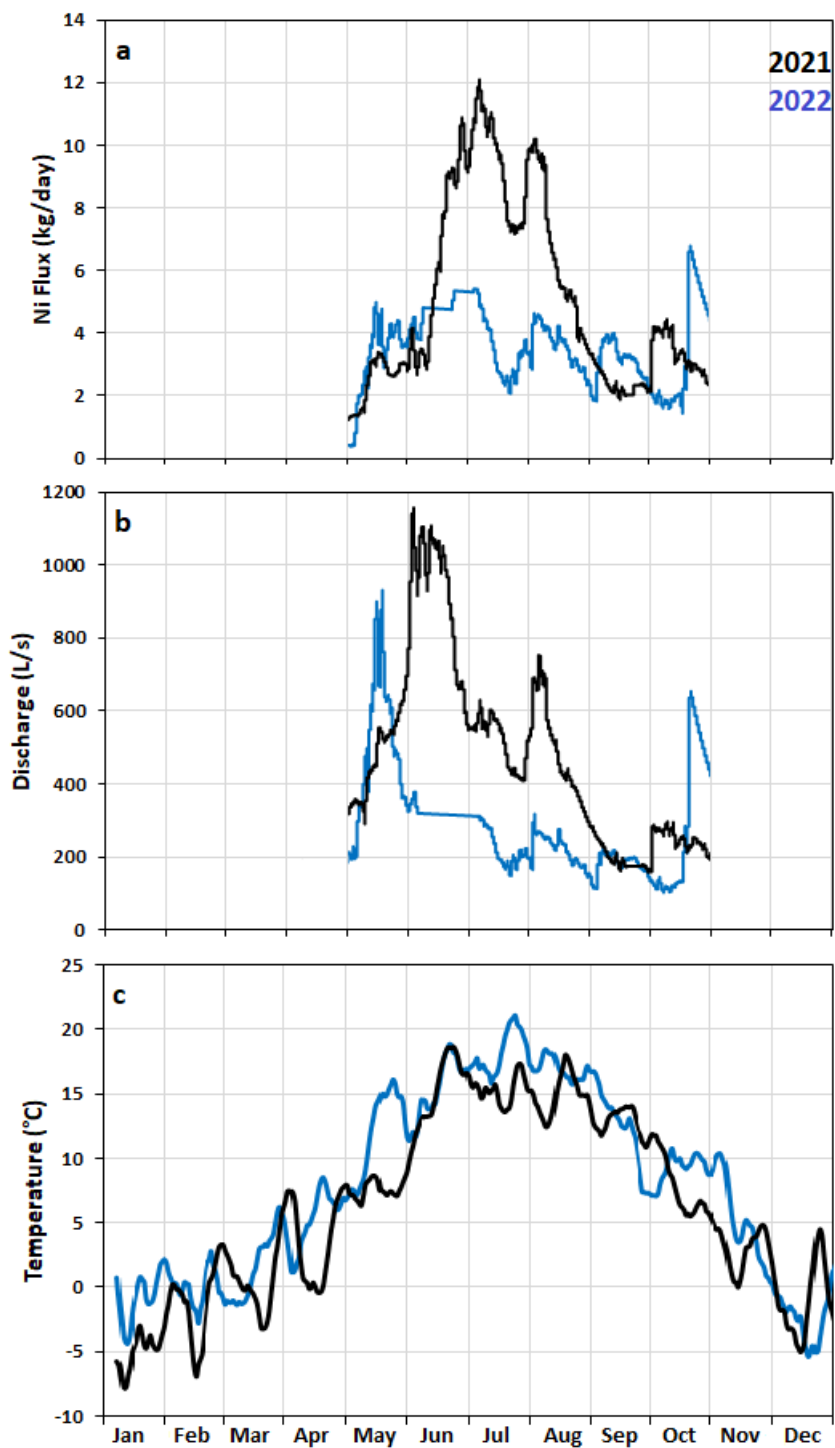
Figure 9: Comparison of selected parameters between the two monitoring years. (a) Ni fluxes estimated at AP10; (b) Discharge at AP10. (C) Daily average temperature at the MeteoSwiss weather station at St. Maria (MeteoSwiss, 2023)**.**

The reasons for the highly prominent role of water infiltration on controlling the export of both toxic solutes and ice melt is
455   illustrate by the conceptual models for element enrichment and their subsequent mobilization shown on Fig. 10. The current understanding of rock glacier hydrology is that the movement of subsurface water follows two distinct flow paths. In Fig. 10, these are referred to as "quick flow" and "base flow," which occur within the active layer (AL) and the base layer (BL), respectively (Giardino et al., 1992; Krainer and Mostler, 2002; Jones et al., 2019). Additionally, subsurface flow through the frozen core (i.e. the sediment-ice mixture), known as intra-flow or slow internal flow, was discovered through dye-tracing
460   experiments (Tenthorey, 1992). Furthermore, as reported for the Lazaun rock glacier, temperatures at or even above 0 °C can be observed towards the top of frozen rock glacier core (Krainer et al., 2015; Nickus et al., 2023), indicating the presence of liquid water promoting intra-permafrost flow. Such fluid flow has been mainly documented in the frontal sections of active rock glaciers which has significant implications on rates of creep and stability of rock glaciers (Jones et al., 2019 and the references therein). In turn, the deformation of rock glacier cores leads to the formation of networks of air voids and
465   fractures, providing positive feedback on intra-permafrost fluid flow.

The presence of liquid water in the rock glacier core is a prerequisite for the chemical interaction with the rock glacier sediments (Wanner et al., 2023a). Moreover, it introduces oxygen into the frozen core, promoting the oxidation of pyrite and thus the generation of sulfuric acid as main weathering agent. If the amount of liquid water is limited and no fully connected
470   water film can develop (Fig. 10a), the toxic elements mobilized from the sediments remain within the rock glacier and their concentrations in the rock glacier spring remain low. Owing to recurring cycles of freezing and thawing within the sediment-ice mixture, with time this leads to a continuous enrichment and interim storage of the leached elements in the rock glacier ice. We hypothesize that this scenario is at play at high altitude or under colder climatic conditions than today, where the amount of ice in the rock glacier is stable. However, more research is required on how much time for the enrichment of toxic
475   elements in the rock glacier ice is needed to cause the high solute concentrations currently observed in the studied rock glacier springs. If the climatic conditions are too cold for seasonal temperatures at or above 0 °C, the rock glacier core is chemically inert, and the accumulation of elements pauses.

In the past years, climate warming likely led to an increase of the time when the temperature at the top of the frozen core of
480   the studied rock glacier is at or above zero. The same applies to the corresponding maximum temperature in summer. Consequently, the amount of liquid water increased, and a fully connected water film has developed towards the top of the rock glacier core (i.e. the top of the sediment-ice mixture). If water from snowmelt and precipitation events reaches the sediment-ice mixture, intra-permafrost flow becomes highly significant and the water film is exported from the rock glacier system. We hypothesize that such hydraulic mobilization of the stagnant water film developed in response to climate

485   warming is the main reason why the amount of water infiltrating into rock glaciers has such a strong control on the export of ice melt produced in the studied rock glacier. Furthermore, owing to the high heat capacity of water, the infiltration of water into the system brings thermal energy to the rock glacier core, further promoting the degradation of the sediment-ice matrix in addition to the hydraulic effect described above. This is particularly relevant under increased intra-permafrost flow where the contact area between the ice and water is elevated. For the studied rock glacier in Val Costainas, the degradation of the

490   rock glacier ice is significant enough to cause a disproportionally high discharge at the monitoring site AP5, located a few hundred meters downstream of the rock glacier (Table 1). Given that there are other rock glaciers in the Val Costainas catchment (Fig. 1a) and that the catchment is widely covered with other quaternary landforms such as talus, moraines, and alluvial cones characterized by significant water storage capacities (Arnoux et al., 2020, 2021), the strongly elevated discharge contribution at AP5 is quite remarkable. While it confirms the general potential of rock glaciers for subsurface

495   water storage (Wagner et al., 2020; 2021b), it demonstrates that the rock glacier at the origin of Aua da Prasüra is currently very active hydraulically.

Since the frozen rock glacier core is heavily enriched with toxic elements, the coupled hydraulic-thermal degradation of the rock glacier ice is manifested by high concentrations in the lowest rock glacier spring AP1 (Fig. 6). In contrast, under dry

500   conditions, the frozen rock glacier core is insulated from the hot summer temperatures at the surface (Hanson and Hoelzle, 2004; Humlum, 1997) and stagnant water films are protected from water-driven export. As a consequence, under dry conditions the export of both ice melt and toxic elements remain rather low such as observed in 2022 (Figs. 8,9).

The different modes for element enrichment and their subsequent mobilization (Fig. 10) reflect the variation of toxic element

505   concentrations in the different rock glacier springs sampled in this study. The lowest concentrations are observed in the AP3 spring discharging at the highest elevation (2770 m a.s l. Table 2). Here, the temperature is still too low to generate a continuous water film in summer. Accordingly, the situation at this spring corresponds to that shown in Fig. 10a where export of ice melt, discharge and toxic element concentrations are low. With decreasing elevation, export of ice melt and hence the concentrations of toxic elements as well as the discharge strongly increase. At the AP1 spring, located at an

510   altitude of 2660 m a.s.l. (Figs. 1,2) the situation corresponds to that shown in Fig. 10b and toxic element concentrations reach maximum values exceeding drinking water limits by factors of up to 226 (Table 2).
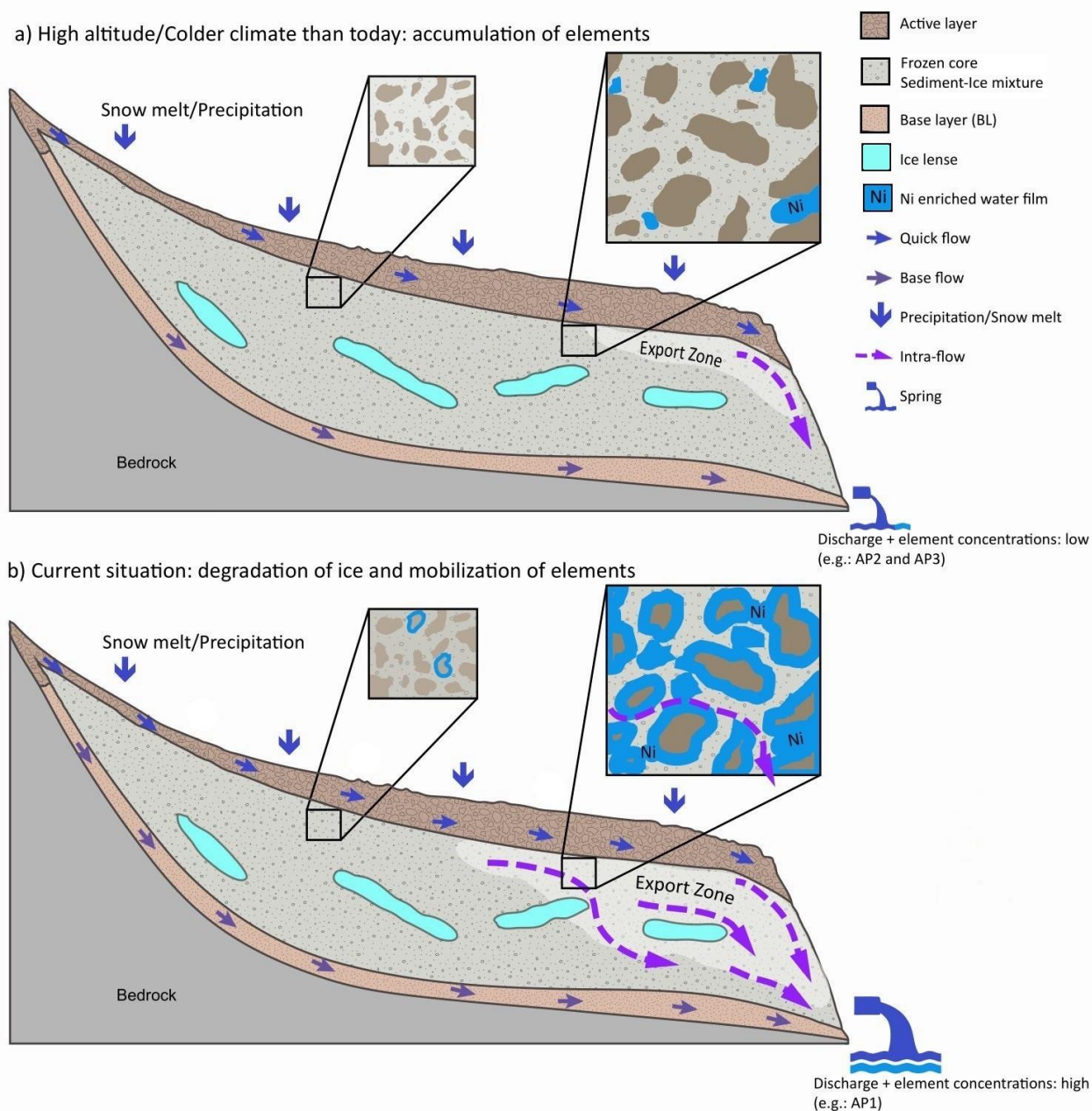
Figure 10: Conceptual models of the coupled thermal-hydraulic-chemical reactions leading to the enrichment of toxic elements in rock glacier ice and the subsequent mobilization into the downhill streams in systems affected by acid rock drainage. (a) Accumulation of elements at high altitude or during climatic conditions where only small parts of the frozen rock glacier core (i.e. the sediment-ice mixture) are seasonally at or even above 0 °C, and where the amount of ice in the rock glacier is stable, (b) Strong element mobilization during permafrost degradation such as today.

515

5.3 Quantifying the export of ice melt from rock glaciers

In addition to gaining novel insights into the coupled process controlling the export of ice melt from rock glaciers, the temporal storage of toxic solutes in rock glacier ice may allow to quantify the actual export of ice melt. While the relative changes of mobilized fluxes directly correspond to the relative changes in the export rates, the estimation of absolute values is more challenging. It is only possible if the following two conditions are met, (i) occurrence of constant concentrations of the enriched elements in the rock glacier ice, and (ii) knowledge about their actual concentrations in the rock glacier ice. If both conditions are met, the ice melt contribution at downstream sampling locations can be estimated based on seasonal concentration curves such as shown in Fig. 8a,b using a binary mixing model:

$$Ice\ melt\ contribution\ (\%) = (X_t / X_{endmember}) * 100 \qquad (2)$$
$$Ice\ melt\ (L\ s^{-1}) = Ice\ melt\ contribution * Q_t \qquad (3)$$

Where X_t is the concentration of the solute of interest at time t (mg L^{-1}), $X_{endmember}$ is the concentration of the solute in the ice (the endmember), and Q_t is the discharge at time t.

While determining the concentration of elements in rock glacier ice feasible by drilling into these landforms and subsequently analyzing the melted ice (Nickus et al., 2023), the prerequisite of having constant concentration in the ice is unlikely to be met. In fact, Nickus et al. (2023) have shown that there are rather strong variations of toxic element concentrations along the frozen core retrieved from the Lazaun rock glacier. Nevertheless, the highest concentrations were observed towards the top of the sediment-ice mixture where the temperature is seasonally at or even above 0 °C. According to the conceptual model, this is exactly the location where most of the ice melt export occurs (i.e. the Export Zone as shown in Fig. 10). Accordingly, determining the average element concentrations in this uppermost part of frozen rock glacier cores might be representative for the element concentration of the meltwater. Therefore, these concentrations could be used for obtaining meaningful estimates of the amount of ice melt being exported from rock glaciers based on toxic solute concentrations continuously measured in the downhill streams.

To test the proposed approach for the studied system, we took the seasonal variation of the concentrations of Ni and Zn at AP10 (Fig. 5). In the absence of drillcores, we further estimated the concentration of both elements in the rock glacier ice by taking their highest concentration measured at the AP1 rock glacier spring (Fig. 1), which are 3.3 and 7.8 mg L^{-1}, respectively. This resulted in the seasonal ice melt export curves shown in Fig. 11. For the May to October monitoring period in 2021, integrating these curves resulted in a total export of ice melt of 283'676 m³ based on Ni and 326'586 m³ for Zn. For 2022, the integration resulted in a total export of 195'425 m³ based on Ni and 234'635 m³ based on Zn.

We consider the fact that similar ice melt export rates are obtained for a specific monitoring year when using different elements for the quantification (2021: ± 15 %; 2022: ± 17 %) as a proof of concept that the proposed approach works. The same applies for the observation that the relative variation of the estimated ice melt export rates between the two monitoring years is very similar than the variation of the corresponding annual element fluxes (both ca. 30 % lower in 2022 than in 2021, *c.f.* Figs. 8a,b). It follows that tracking element fluxes downstream of intact rock glaciers allows obtaining reliable estimates of the relative variation of ice melt export rates without knowing the concentration of the elements in the rock glacier ice.

In contrast, the estimated amounts of total ice melt exported from the studied rock glacier per monitoring period (Fig. 11) are strongly overestimated because the concentrations in AP1 are certainly lower than the maximum concentration in the rock glacier ice. This is manifested by relating the estimated export rates to the surface area of the studied rock glacier (40'000 m^2). In the two monitoring years, the average yearly export of ice melt obtained from the two elements correspond to a degradation of 7.5 (2021) and 5.3 m (2022). Considering that Krainer et al. (2015) estimated an annual rock glacier ice degradation of about 10 centimeters, our estimates are at least one order of magnitude too high. The overestimation likely reflects the degree of dilution between the rock glacier ice and AP1. This is consistent with data from the Lazaun rock glacier ice, where the concentrations of Ni, and Zn in the rock glacier ice are about 10 times higher than in the corresponding rock glacier spring (Nickus et al., 2023). This confirms that reliable estimates may be obtained when drilling into the rock glacier and determining the concentrations of elements enriched in the rock glacier ice.

Overall, our data demonstrate the great potential of the strong chemical signal observed in springs discharging from intact rock glaciers affected by ARD to continuously track the relative and maybe even the absolute amounts of ice melt exported from rock glaciers. Installing multiple monitoring stations at different rock glaciers could thus help to obtain more insights on regional and maybe even global ice melt export rates in rock glacier systems. In a first step, such effort should focus on systems affected by ARD because of their strong chemical signal, which allow estimating the fluxes at distant downstream locations more accessible for continuous sampling and measurements than the actual rock glacier springs. Future research, however, should also focus on systems not affected by ARD in order to assess whether an enrichment of solutes in ice is also detectable in chemically less reactive systems and subsequently used for quantifying the export of ice melt.
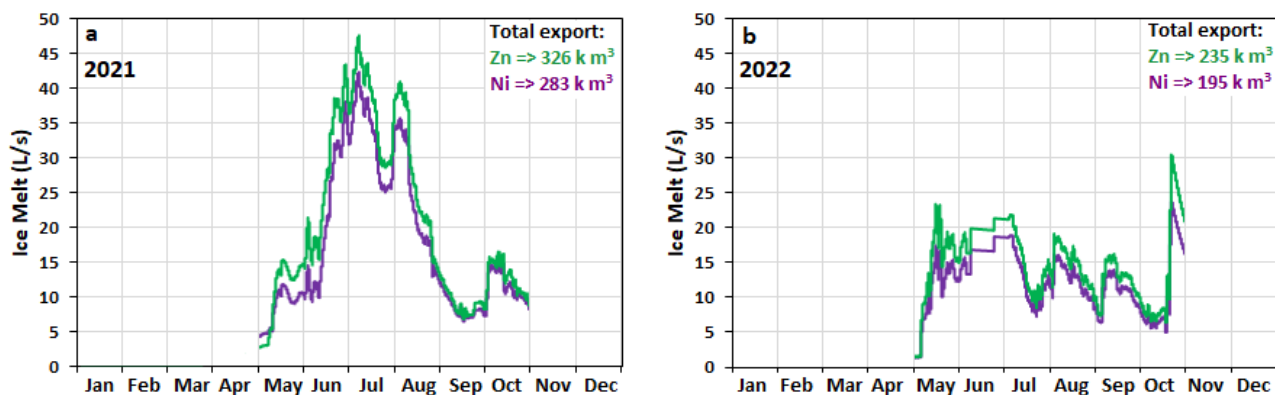
Figure 11: Estimates of seasonal evolution of ice melt exported from the rock glacier at the origin of Aua da Prasüra estimated based on the fluxes of Ni and Zn at AP10 and the corresponding maximum concentrations in the rock glacier spring at AP1. (a) 2021, (b) 2022.

6 Conclusions

The detailed, two-year long monitoring of a high-alpine stream affected by acid rock drainage (ARD) in Eastern Switzerland provided novel insights on the causes for the massive mobilization of toxic solutes such as Al, F⁻, Zn, Mn, and Ni from an intact rock glacier located at the origin of the stream. The main conclusions and implications for the future are listed below:

- Very high concentrations of Al, F⁻, Zn, Mn, and Ni are observed at the rock glacier spring located at the lowest altitude, exceeding drinking water limits by factors of up to 226. At 5 km downstream, these concentrations still exceed the drinking water limits by factors of up to 15. Given that the surface area of the studied rock glacier only covers an area of around 40'000 m², the fluxes of these solutes are remarkably high, reaching up to several tons per year.

- The presence of liquid water in the rock glacier core is required for the production of sulfuric acid as weathering agent, promoting the dissolution of the toxic solutes from the host rock. Moreover, it introduces oxygen, accelerating pyrite weathering. In the past, recurring cycles of freezing and thawing within the sediment-ice mixture (i.e. the rock glacier core), has led to the enrichment and interim storage of the leached solutes in the rock glacier ice.

- Today, climate warming increases the temperature of the top of the frozen core, causing the formation of a continuous water film at the interface between sediments and ice. Infiltration of water from snow melt and precipitation leads to a quick hydraulic export of the water film from the rock glacier causing export of both ice melt and toxic solutes. This is manifested by the strong positive correlation between solutes fluxes and the discharge.

- In the studied system, the export of ice melt from the rock glaciers currently causes a disproportionally high discharge in summer, confirming that rock glaciers will play a more important role as water resources in alpine regions.

610
- The fluxes of toxic elements exported from intact rock glaciers affected by ARD are likely to increase until reaching a maximum. More research is required to estimate when this will be reached and what the maximum concentrations and fluxes would be. This increase in the toxic element concentrations correspond to a decline in water quality downstream of rock glaciers impacted by ARD, emphasizing the necessity for continuous monitoring of such systems.

- This strong chemical signal provides the opportunity to quantify the amount of ice melt exported from rock glaciers.
615
Our data demonstrate that relative changes in element fluxes correspond to relative changes in the export rates of ice melt. Moreover, it demonstrates that determining the absolute export rates of ice melt would be feasible if the concentrations of solutes in the rock glacier ice were known. Consequently, monitoring solute fluxes exported from rock glaciers is a promising future research direction for obtaining more reliable estimates of the amount ice melt exported from rock glaciers.

620 **Data availability**

Research data can be accessed at https://zenodo.org/doi/10.5281/zenodo.10558549 (Moradi et al., 2024).

Author contribution

HM and CW designed the study. HM, CW, GF, and MM carried out the sampling and monitoring campaigns. HM, performed the chemical analyses of streamwater. HM and CW analyzed the data. HM with supervision of CW wrote the
625 original draft. DM planned the UAV survey and prepared the figures showing maps. CW, GF, DM, and MM reviewed and edited the draft. CW acquired funding and was responsible for project management.

Competing interests

The contact author has declared that none of the authors has any competing interests.

Acknowledgements

630 We express our gratitude to Priska Bähler, Philipp Hänggi, and Christopher Pichler for their support in the chemical analyses of streamwater. Special appreciation goes to Linda Feichtinger and her team from Biosfera Val Müstair for their dedicated efforts in conducting bi-weekly water sampling. We also thank Marco Ferrari and David Schmid from the Amt für Natur und

Umwelt, Canton of Graubünden (ANU) for maintaining the combined water table and electric conductivity probe used in this study.

Financial support

This research was funded by the Swiss National Science Foundation is greatly appreciated (SNSF Grant 196847 to CW).

References

ANU: https://www.gr.ch/DE/institutionen/verwaltung/ekud/anu/aktuelles/umweltbeobachtung/hydrodaten/Seiten/Hydrodaten.aspx #/device/UMBRAIL_20/pegel_m, last access: 11 January 2024.

Arnoux, M., Halloran, L. J. S., Berdat, E., and Hunkeler, D.: Characterizing seasonal groundwater storage in alpine catchments using time-lapse gravimetry, water stable isotopes and water balance methods, Hydrol. Process., 34, 4319–4333, https://doi.org/10.1002/hyp.13884, 2020.

Arnoux, M., Brunner, P., Schaefli, B., Mott, R., Cochand, F., and Hunkeler, D.: Low-flow behavior of alpine catchments with varying quaternary cover under current and future climatic conditions, J. Hydrol., 592, 125591, https://doi.org/10.1016/j.jhydrol.2020.125591, 2021.

Ballantyne, C. K.: Periglacial Geomorphology, John Wiley & Sons Ltd, 2018.

Barsch, D.: Rockglaciers, Springer Berlin, Heidelberg, Berlin, 331 pp., https://doi.org/https://doi.org/10.1007/978-3-642-80093-1, 1996.

Brighenti, S., Tolotti, M., Bruno, M. C., Wharton, G., Pusch, M. T., and Bertoldi, W.: Ecosystem shifts in Alpine streams under glacier retreat and rock glacier thaw: A review, Sci. Total Environ., 675, 542—559, https://doi.org/10.1016/j.scitotenv.2019.04.221, 2019.

Brighenti, S., Engel, M., Tolotti, M., Bruno, M. C., Wharton, G., Comiti, F., Tirler, W., Cerasino, L., and Bertoldi, W.: Contrasting physical and chemical conditions of two rock glacier springs, Hydrol. Process., 35, 1–18, https://doi.org/10.1002/hyp.14159, 2021.

Calkins, D. and Dunne, T.: A salt tracing method for measuring channel velocities in small mountain streams, J. Hydrol., 11, 379–392, https://doi.org/https://doi.org/10.1016/0022-1694(70)90003-X, 1970.

Colombo, N., Gruber, S., Martin, M., Malandrino, M., Magnani, A., Godone, D., Freppaz, M., Fratianni, S., and Salerno, F.: Rainfall as primary driver of discharge and solute export from rock glaciers: The Col d'Olen Rock Glacier in the NW Italian Alps, Sci. Total Environ., 639, 316–330, https://doi.org/10.1016/j.scitotenv.2018.05.098, 2018.

Day, T. J.: Observed mixing lengths in mountain streams, J. Hydrol., 35, 125–136, https://doi.org/https://doi.org/10.1016/0022-1694(77)90081-6, 1977.

Diem, D. and Stumm, W.: Is dissolved Mn2+ being oxidized by O2 in absence of Mn-bacteria or surface catalysts?, Geochim. Cosmochim. Acta, 48, 1571–1573, https://doi.org/https://doi.org/10.1016/0016-7037(84)90413-7, 1984.

Giardino, J. R. and Vitek, J. D.: The significance of rock glaciers in the glacial-periglacial landscape continuum, J. Quat. Sci., 3, 97–103, https://doi.org/https://doi.org/10.1002/jqs.3390030111, 1988.

Giardino John R, Vitek John D, D. J. L.: Periglacial Geomorphology, in: A Model of Water Movement in Rock Glaciers and Associated Water Characteristics, 26, https://doi.org/https://doi.org/10.4324/9781003028901, 1992.

Hanson, S. and Hoelzle, M.: The thermal regime of the active layer at the Murtèl rock glacier based on data from 2002,

670 Permafr. Periglac. Process., 15, 273–282, https://doi.org/10.1002/ppp.499, 2004.

Hauck, C.: New concepts in geophysical surveying and data interpretation for permafrost terrain, Permafr. Periglac. Process., 24, 131–137, https://doi.org/10.1002/ppp.1774, 2013.

Hauck, C., Böttcher, M., and Maurer, H.: A new model for estimating subsurface ice content based on combined electrical and seismic data sets, Cryosphere, 5, 453–468, https://doi.org/10.5194/tc-5-453-2011, 2011.

675 Humlum, O.: Active layer thermal regime at three rock glaciers in Greenland, Permafr. Periglac. Process., 8, 383–408, https://doi.org/10.1002/(sici)1099-1530(199710/12)8:4<383::aid-ppp265>3.0.co;2-v, 1997.

Ilyashuk, B. P., Ilyashuk, E. A., Psenner, R., Tessadri, R., and Koinig, K. A.: Rock glacier outflows may adversely affect lakes: Lessons from the past and present of two neighboring water bodies in a crystalline-rock watershed, Environ. Sci. Technol., 48, 6192–6200, https://doi.org/10.1021/es500180c, 2014.

680 Jones, D. B., Harrison, S., Anderson, K., and Betts, R. A.: Mountain rock glaciers contain globally significant water stores, Sci. Rep., 8, 1–10, https://doi.org/10.1038/s41598-018-21244-w, 2018.

Jones, D. B., Harrison, S., Anderson, K., and Whalley, W. B.: Rock glaciers and mountain hydrology: A review, https://doi.org/10.1016/j.earscirev.2019.04.001, 1 June 2019.

Kenner, R., Noetzli, J., Hoelzle, M., Raetzo, H., and Phillips, M.: Distinguishing ice-rich and ice-poor permafrost to map 685 ground temperatures and ground ice occurrence in the Swiss Alps, Cryosphere, 13, 1925–1941, https://doi.org/10.5194/tc-13-1925-2019, 2019.

Krainer, K. and Mostler, W.: Hydrology of Active Rock Glaciers: Examples from the Austrian Alps, Arctic, Antarct. Alp. Res., 34, 142–149, https://doi.org/10.1080/15230430.2002.12003478, 2002.

Krainer, K., Mostler, W., and Spötl, C.: Discharge from active rock glaciers, Austrian Alps: A stable isotope approach, 690 Austrian J. Earth Sci., 100, 102–112, 2007.

Krainer, K., Bressan, D., Dietre, B., Haas, J. N., Hajdas, I., Lang, K., Mair, V., Nickus, U., Reidl, D., Thies, H., and Tonidandel, D.: A 10,300-year-old permafrost core from the active rock glacier Lazaun, southern Ötztal Alps (South Tyrol, northern Italy), Quat. Res. (United States), 83, 324–335, https://doi.org/10.1016/j.yqres.2014.12.005, 2015.

Leibundgut, C., Maloszewski, P., and Külls, C.: Tracers in Hydrology, Tracers Hydrol., 1–415, 695 https://doi.org/10.1002/9780470747148, 2009.

Li, M., Yang, Y., Peng, Z., and Liu, G.: Assessment of rock glaciers and their water storage in Guokalariju, Tibetan Plateau, Cryosphere, 18, 1–16, https://doi.org/10.5194/tc-18-1-2024, 2024.

Maillet, E.: Essais d'Hydraulique souterraine et fluviale, Nature, 72, 25–26, 1905.

Mark, B. G. and Mckenzie, J. M.: Tracing increasing tropical Andean glacier melt with stable isotopes in water, Environ. 700 Sci. Technol., 41, 6955–6960, https://doi.org/10.1021/es071099d, 2007.

MeteoSwiss: https://www.meteoschweiz.admin.ch/service-und-publikationen/applikationen/messwerte-und-messnetze.html#lang=de&swisstopoApiKey=cpZJOL3HuO5yENksi97q¶m=messwerte-niederschlag-10min&station=SMM&chart=month, last access: 11 January 2024.

Mewes, B., Hilbich, C., Delaloye, R., and Hauck, C.: Resolution capacity of geophysical monitoring regarding permafrost 705 degradation induced by hydrological processes, Cryosphere, 11, 2957–2974, https://doi.org/10.5194/tc-11-2957-2017, 2017.

Moradi, H., Furrer, G., Michael, M., David, M., and Wanner, C.: Massive mobilization of toxic elements from an intact rock glacier in the Central Eastern Alps: insights on ice melt dynamics, https://doi.org/https://zenodo.org/doi/10.5281/zenodo.10558549, 2024.

Munroe, J. S. and Handwerger, A. L.: Contribution of rock glacier discharge to late summer and fall streamflow in the Uinta 710 Mountains, Utah, USA, Hydrol. Earth Syst. Sci., 27, 543–557, https://doi.org/10.5194/hess-27-543-2023, 2023.

Nickus, U., Thies, H., Krainer, K., Lang, K., Mair, V., and Tonidandel, D.: A multi-millennial record of rock glacier ice

chemistry (Lazaun, Italy), Front. Earth Sci., 11, https://doi.org/10.3389/feart.2023.1141379, 2023.

Noetzli, J. and Pellet, C. (eds. .: PERMOS, Swiss Permafrost Bulletin 2022, 23 pp., https://doi.org/Available at: https://www.permos.ch/publications, 2023.

715 Schmid, S. M., Fügenschuh, B., Kissling, E., and Schuster, R.: Tectonic map and overall architecture of the Alpine orogen, Eclogae Geol. Helv., 97, 93–117, https://doi.org/10.1007/s00015-004-1113-x, 2004.

Schmid, S. V: Geologie des Umbrailgebiets, 66, 101–210, https://doi.org/http://dx.doi.org/10.5169/seals-164185, 1973.

SLF: https://www.slf.ch/de/lawinenbulletin-und-schneesituation/messwerte/beschreibung-automatische-stationen/, last access: 11 January 2024.

720 Swisstopo: https://shop.swisstopo.admin.ch/en/maps/geological-maps/explanatory-booklet-geological-atlas-switzerland-25000, last access: 11 January 2024a.

Swisstopo: https://www.swisstopo.admin.ch/en/geodata/geology/maps/geocover.html, last access: 11 January 2024b.

Tenthorey, G.: Perennial névés and the hydrology of rock glaciers, Permafr. Periglac. Process., 3, 247–252, https://doi.org/10.1002/ppp.3430030313, 1992.

725 Thies, H., Nickus, U., Mair, V., Tessadri, R., Tait, D., Thaler, B., and Psenner, R.: Unexpected response of high alpine lake waters to climate warming, Environ. Sci. Technol., 41, 7424–7429, https://doi.org/10.1021/es0708060, 2007.

Todd, A. S., Manning, A. H., Verplanck, P. L., Crouch, C., McKnight, D. M., and Dunham, R.: Climate-change-driven deterioration of water quality in a mineralized watershed, Environ. Sci. Technol., 46, 9324–9332, https://doi.org/10.1021/es3020056, 2012.

730 Wagner, T., Brodacz, A., Krainer, K., and Winkler, G.: Active rock glaciers as shallow groundwater reservoirs, Austrian Alps, Grundwasser, 25, 215–230, https://doi.org/10.1007/s00767-020-00455-x, 2020.

Wagner, T., Seelig, S., Helfricht, K., Fischer, A., Avian, M., Krainer, K., and Winkler, G.: Assessment of liquid and solid water storage in rock glaciers versus glacier ice in the Austrian Alps, Sci. Total Environ., 800, 149593, https://doi.org/10.1016/j.scitotenv.2021.149593, 2021a.

735 Wagner, T., Kainz, S., Krainer, K., and Winkler, G.: Storage-discharge characteristics of an active rock glacier catchment in the Innere Ölgrube, Austrian Alps, Hydrol. Process., 35, 1–16, https://doi.org/10.1002/hyp.14210, 2021b.

Wanner, C., Pöthig, R., Carrero, S., Fernandez-Martinez, A., Jäger, C., and Furrer, G.: Natural occurrence of nanocrystalline Al-hydroxysulfates: Insights on formation, Al solubility control and As retention, Geochim. Cosmochim. Acta, 238, 252–269, https://doi.org/10.1016/j.gca.2018.06.031, 2018.

740 Wanner, C., Moradi, H., Ingold, P., Cardenas Bocanegra, M. A., Mercurio, R., and Furrer, G.: Rock glaciers in the Central Eastern Alps – How permafrost degradation can cause acid rock drainage, mobilization of toxic elements and formation of basaluminite, Glob. Planet. Change, 227, https://doi.org/10.1016/j.gloplacha.2023.104180, 2023a.

Wanner, P., Zischg, A., and Wanner, C.: Quantifying the glacial meltwater contribution to mountainous streams using stable water isotopes: What are the opportunities and limitations?, Hydrol. Process., 37, 1–14, https://doi.org/10.1002/hyp.14963,
745 2023b.

Williams, M. W., Knauf, M., Caine, N., Liu, F., and Verplanck, P. L.: Geochemistry and source waters of rock glacier outflow, Colorado Front Range, Permafr. Periglac. Process., 17, 13–33, https://doi.org/10.1002/ppp.535, 2006.

Zarroca, M., Roqué, C., Linares, R., Salminci, J. G., and Gutiérrez, F.: Natural acid rock drainage in alpine catchments: A side effect of climate warming, Sci. Total Environ., 778, 146070, https://doi.org/10.1016/j.scitotenv.2021.146070, 2021.

750